Inorg. Chem. **2009**, *48*, 946−952

Dimensionally Modulated, Single-Crystalline $LiMPO_4$ (M= Mn, Fe, Co, and Ni) with Nano-Thumblike Shapes for High-Power Energy Storage

A. Vadivel Murugan, T. Muraliganth, P. J. Ferreira, and A. Manthiram*

Electrochemical Energy Laboratory & Materials Science and Engineering Program, The University of Texas at Austin, Austin, Texas 78712, USA

Received August 18, 2008

We demonstrate an efficient and rapid microwave irradiated solvothermal method to prepare nanostructured lithium metal phosphates $LiMPO_4$ (M = Mn, Fe, Co, and Ni) within a short reaction time (5−15 min) at temperatures as low as 300 °C without requiring any post annealing at elevated temperatures. The highly viscous, high-boiling tetraethyleneglycol used as the solvent not only provides a reducing atmosphere to prevent the oxidation of M^{2+} to M^{3+} but also inhibits the agglomeration of the nanoparticles formed. The enhanced reaction rates facilitated by the dielectric volumetric heating of the microwave absorbing reactants led to the formation of highly crystalline, phase-pure $LiMPO_4$ powders. The samples are characterized by X-ray diffraction, Raman spectroscopy, transmission electron microscopy (TEM), and electrochemical measurements in lithium cells. High-resolution TEM studies reveal the formation of single-crystalline $LiMPO_4$ with nano-thumblike shapes. The dimensionally modulated nano-thumblike shapes with the lithium diffusion direction (*b* axis) along the shorter dimension are particularly beneficial to achieve high-power capability in lithium ion cells. Subsequent networking of the single-crystalline $LiMPO_4$ nano-thumps with multiwalled carbon nanotubes by a simple solution-based mixing at ambient temperatures to overcome the electronic conductivity limitations offers excellent electrochemical performance in lithium ion cells.

1. Introduction

Lithium ion batteries have played a key role in the portable electronics revolution, and the technology is now being vigorously pursued for vehicle applications. The major challenges in adopting the technology for vehicle applications are the safety concerns arising from the chemical instability at deep charge as well as the high cost of the currently used layered $LiCoO_2$ cathode. Whereas highly oxidized redox couples such as $Co^{3+/4+}$ and $Ni^{3+/4+}$ are generally desired in simple oxides like $LiCoO_2$ to maximize the cell voltage in lithium ion cells, they invariably lead to chemical instability and safety concerns. Recognizing this, oxides with polyanions like $(XO_4)^{2-}$ (X = S, Mo, and W) were first initiated by Manthiram and Goodenough[1,2] as lithium insertion/extraction hosts in the late 1980s because the covalently bonded groups like $(SO_4)^{2-}$ can lower the redox energies of lower-valent, chemically more stable couples like $Fe^{2+/3+}$ through inductive effect and increase the cell voltage. Following this, the lithium transition-metal phosphates $LiMPO_4$ (M = Mn, Fe, Co, Ni) crystallizing in the olivine structure were identified by Padhi et al.[3] in the 1990s as potential cathodes for lithium ion cells.

Among these compounds, $LiFePO_4$ has drawn considerable attention as Fe is inexpensive and environmentally benign, and the covalently bonded PO_4 groups together with the chemically more stable $Fe^{2+/3+}$ couple offer excellent thermal stability and safety.[3,4] Moreover, with a theoretical capacity of 170 mAh/g, $LiFePO_4$ operates at a flat voltage of 3.45 V versus Li/Li^+, which is compatible with the commercial electrolytes used now in lithium ion batteries. On the other hand, the other $LiMPO_4$ cathodes with $Mn^{2+/3+}$, $Co^{2+/3+}$, and $Ni^{2+/3+}$ couples have been shown to operate at much higher voltages of respectively, 4.1, 4.8, and 5.1 V,[5−7] offering the potential to increase the energy and power density. However,

* To whom correspondence should be addressed. E-mail: rmanth@mail.utexas.edu. Phone: 512-471-1791. Fax: 512-471-7681.

(1) Manthiram, A.; Goodenough, J. B. *J. Solid State Chem.* **1987**, *71*, 349.
(2) Manthiram, A.; Goodenough, J. B. *J. Power Sources* **1989**, *26*, 403.
(3) Padhi, A. K.; Nanjundasawamy, K. S.; Goodenough, J. B. *J. Electrochem. Soc.* **1997**, *144*, 1188.
(4) Koltypin, M.; Aurbach, D.; Nazar, L.; Ellis, B. *Electrochem. Solid-State Lett.* **2007**, *10*, A40.
(5) Yang, J.; Xu, J. J. *J. Electrochem. Soc.* **2006**, *153*, A716.
(6) Zhou, F.; Cococcioni, M.; Kang, K.; Ceder, G. *Electrochem. Commun.* **2004**, *6*, 1144.

10.1021/ic8015723 CCC: $40.75
Published on Web 01/06/2009

the major drawback with the $LiMPO_4$ cathodes is the poor lithium ion and electronic conductivity. Tremendous efforts have been made in recent years to overcome these problems by cationic doping,[8−10] decreasing the particle size through various synthesis methods,[11−17] and coating with electronically conducting agents.[17−20] Particularly, nanosize $LiFePO_4$ particles have been shown to exhibit excellent performance with high rate capability due to a shortening of both the electron and lithium ion diffusion path lengths within the particles.[13,16] In this regard, dimensionally modulated nanostructures such as nanorods, nanowires, and nanosheets are appealing as they can efficiently transport charge carriers while maintaining a large surface to volume ratio, enhancing the contact with the electrolyte and the reaction kinetics.

Among the various synthesis approaches pursued in the past few years, solution-based methods have been particularly successful for $LiFePO_4$ with respect to controlling the chemical composition, tailoring the crystallite size, and particle morphologies. However, these methods require either long reaction times (5−24 h)[11−15,21] or further post heat treatment processing at temperatures as high as 700 °C in reducing atmospheres to achieve phase-pure samples and a high degree of crystallinity.[11,14,15] In this regard, microwave-assisted synthesis approaches are extremely appealing as they can shorten the reaction time from several hours to a few minutes with enormous energy savings and cleanliness.[22,23] The microwave-assisted solvothermal (MW-ST) approach offers several advantages compared to the conventional solvothermal or hydrothermal approaches, which suffer from slow reaction kinetics and nonuniform reaction conditions because of sharp thermal gradients inside the bulk solution.[24] Whereas the solvothermal and hydrothermal methods rely on convective heating of the reactants, the MW-ST method utilizes dielectric microwave heating of the total volume of the reactants by transferring energy selectively to microwave absorbing materials, which reduces thermal gradients inside the reaction vessel. Thus, the MW-ST method is advantageous for large-scale industrial production as it provides a uniform nucleation environment and offers highly crystalline monodispersed nanocrystals of high quality within a short reaction time.[17,25]

In this context, we present here a rapid (5−15 min), straightforward synthesis of $LiMPO_4$ (M = Mn, Fe, Co, Ni) with nano-thumblike shapes using the highly viscous, high boiling tetraethyleneglycol (TEG) solvent via the MW-ST method at temperatures as low as 300 °C. Moreover, the as-synthesized $LiFePO_4$, $LiMnPO_4$, and $LiCoPO_4$ samples are subsequently networked with multiwalled carbon nanotubes (MWCNT) by a simple, ambient-temperature procedure to overcome the poor electronic conductivity limitations of $LiMPO_4$ without requiring any post annealing at elevated temperatures. This nanoscale networking with MWCNT enhances the mobility of electrons between the adjacent $LiMPO_4$ particles during the lithiation/delithiation process without blocking the lithium ion transport.

2. Experimental Section

2.1. Microwave-Solvothermal (MW-ST) Synthesis of $LiMPO_4$. $LiMPO_4$ (M = Mn, Fe, Co and Ni) nano-thumblike shapes were prepared by a rapid microwave-solvothermal approach as described below. Lithium hydroxide (Fisher) and the respective acetates of Mn, Fe, Co, or Ni [Manganese(II) acetate tetrahydrate (ACROS ORGANICS), iron(II) acetate (GFS-Chemicals), cobalt(II) acetate tetrahydrate (Alfa Aesar), nickel(II) acetate tetrahydrate (ACROS ORGANICS)] were dissolved in tetraethyleneglycol (TEG) (ACROS-Organics) in a quartz vessel suitable to be used in the microwave system. H_3PO_4 (85%, Fisher) was then added dropwise to the reaction mixture at room temperature to realize a Li/M/P molar ratio of 1:1:1. Whereas the reaction mixtures were acidic for M = Mn and Fe, they were kept basic for M = Co and Ni by adding ammonium hydroxide. The homogeneous light-pink gel formed for M = Mn, reddish-brown gel formed for M = Fe, violet gel formed for M = Co, and pale-green gel formed for M = Ni as shown in Scheme 1 were sealed in the closed high-pressure quartz vessels, which were fitted with a pressure and temperature probe housed in a sturdy thermowell and protected from chemical attack. The rotor containing the closed quartz vessels was then placed on a turntable for uniform heating in an Anton Paar microwave synthesis system (*Synthos-3000*). The desired exposure time and temperature were programmed with the Anton Paar, *Synthos-3000* software. The automatic temperature and pressure control system allowed continuous monitoring and control of the internal temperature (±1 °C). The preset profile (desired time, temperature, and pressure) was followed automatically by continuously adjusting the applied power (0−600 W) and pressure (up to 80 bar). The system was operated at a frequency of 2.45 GHz and a power of 600 W, the sample temperature was ramped to 300 °C, and kept at 300 °C for 5 or 15 min under the solvothermal condition. Precipitation of $LiMPO_4$ took place inside the reactor during this solvothermal process, and the reactor was then cooled to room temperature by an in-built cooling fan capability in the *Synthos-3000* system. The supernatant TEG solvent was carefully decanted,

(7) Okada, S.; Sawa, S.; Egashira, M.; Yamaki, J.-I.; Tabuchi, M.; Kageyama, H.; Konicshi, T.; Yoshino, A. *J. Power Sources* **2001**, *97*, 430.
(8) Chung, S.-Y.; Bloking, J. T.; Chiang, Y.-M. *Nat. Mater.* **2002**, *2*, 123.
(9) Liu, H.; Cao, Q.; Fu, L. J.; Li, C.; Wu, Y. P.; Wu, H. Q. *Electrochem. Commun.* **2006**, *8*, 1553.
(10) Shi, S.; Liu, L.; Ouyang, C.; Wang, D.-S.; Wang, Z.; Chen, L.; Huang, X. *Phys. Rev. B* **2003**, *68*, 195108.
(11) Ellis, B.; Kan, W. H.; Makahnouk, W. R. M.; Nazar, L. F. *J. Mater. Chem.* **2007**, *17*, 3248.
(12) Franger, S.; Cras, F. L.; Bourbon, C.; Rouault, H. *J. Power Sources* **2003**, *119−121*, 252.
(13) Gaberscek, M.; Dominko, R.; Jamnik, J. *Electrochem. Commun.* **2007**, *9*, 2778.
(14) Yang, J.; Xu, J. J. *J. Electrochem. Soc.* **2006**, *153*, A716.
(15) Yang, Y.; Xu, J. J. *Electrochem. Solid State Lett.* **2004**, *7*, A515.
(16) Yamada, A.; Chung, S. C.; Hinokuma, K. *J. Electrochem. Soc.* **2001**, *148*, A224.
(17) Vadivel Murugan, A.; Muraliganth, T.; Manthiram, A. *Electrochem. Commun.* **2008**, *10*, 903.
(18) Wang, Y.; Wang, J.; Yang, J.; Nuli, Y. *Adv. Func. Mater.* **2006**, *16*, 2135.
(19) Ravet, N.; Chouinard, Y.; Magnan, J. F.; Besner, S.; Gauthier, M.; Armand, M. *J. Power Sources* **2001**, *97−98*, 503.
(20) Hu, Y. -S.; Guo, Y. -G.; Dominko, R.; Gaberscek, M.; Jamnik, J.; Maier, *J. Adv. Mater.* **2007**, *19*, 1963.
(21) Dokko, K.; Kuizumi, S.; Nakano, H.; Kanamura, K. *J. Mater. Chem.* **2007**, *17*, 4803.
(22) Bilecka, I.; Djerdj, I.; Niederberger, M. *Chem. Commun.* **2008**, 886.
(23) Panda, A. B.; Glaspell, G.; El-Shall, M. S. M. *J. Am. Chem. Soc.* **2006**, *128*, 2790.
(24) Gerbec, J. A.; Magana, D.; Washington, A.; Strouse, G. F. *J. Am. Chem. Soc.* **2005**, *127*, 15791.
(25) Vadivel Murugan, A.; Muraliganth, T.; Manthiram, A. *J. Phys. Chem. C* **2008**, *112*, 14665.

Scheme 1. Schematic Representation of the MW-ST Process to Produce $LiMPO_4$ (M = Mn, Fe, Co, Ni) and Subsequent Nanocomposite Formation with MWCNT at Ambient Temperatures

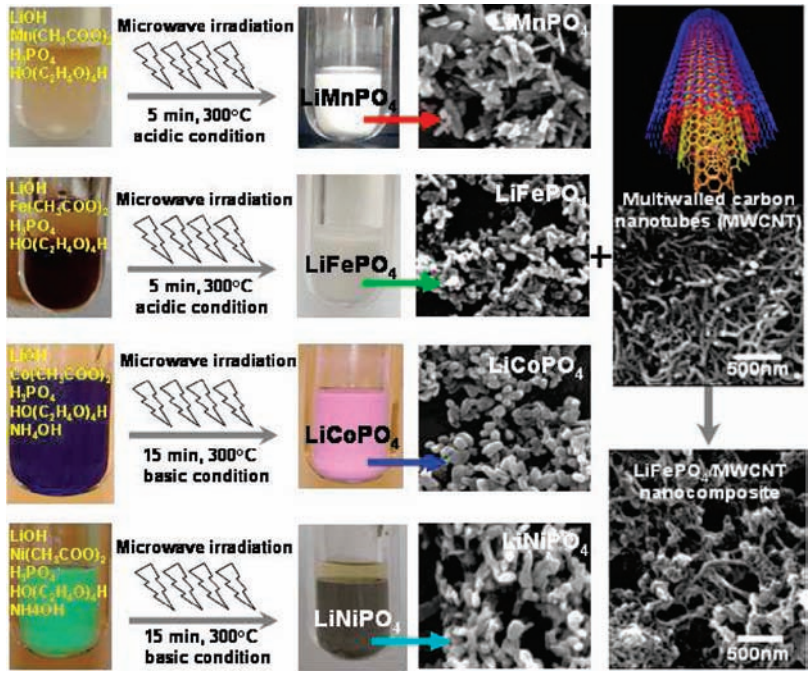

and the resulting carbon free milk-white $LiMnPO_4$, cream-white $LiFePO_4$, pink $LiCoPO_4$, and gray $LiNiPO_4$ were washed repeatedly by acetone until the washings were colorless to ensure the complete removal of TEG. The obtained powder was then dried in a vacuum oven at 250 °C for 1 h. The reactant concentrations were kept at 0.15 M each of Li^+, M^{2+}, and $(PO_4)^{3-}$ in TEG. The samples could be synthesized with good reproducibility since the temperature, microwave power, and reaction time could be controlled easily using the software available with the microwave synthesis system used. Provision to run eight parallel reactions at the same time with the microwave synthesis system allowed us to prepare all the four phospho-olivines with M = Mn, Fe, Co, and Ni in the same batch.

2.2. Synthesis of $LiMPO_4$−MWCNT Nanocomposites. MWCNT with a diameter in the range of 20−30 nm was synthesized by a catalytic chemical vapor deposition (CVD) process at 650 °C in 10% H_2/90% Ar atmosphere, employing a ferrocene−toluene mixture.[26,27] The as-synthesized MWCNTs were refluxed in a 1:1 mixture of 98% H_2SO_4 and 78% HNO_3 for 24 h at 60 °C to oxidize the graphitic sp^2 carbon into −COOH and −OH groups on the side walls of the nanotubes. The acid group functionalized MWCNT was filtered through a polytetrafluoroethylene (PTFE) membrane, washed thoroughly with deionized water, suspended in toluene, and sonicated for a few minutes. An appropriate amount of the MWCNT in toluene was then mixed with the nanostructured $LiMPO_4$ (M = Mn, Fe, and Co) powder synthesized by the microwave-solvothermal process by magnetic stirring for a few minutes at ambient temperature to ensure a complete mixing of the $LiMPO_4$ with MWCNT and the formation of a highly conductive nanonetwork of MWCNT on the nano-thumblike $LiMPO_4$. The mixture was then dried in a vacuum oven at 250 °C for 1 h. The weight percent of $LiMPO_4$ to MWCNT in the mixture was 92:8.

2.3. Structural, Physical, and Chemical Characterizations. XRD characterization of the samples was carried out with a Philips PW1830 X-ray diffractometer using filtered Cu Kα radiation. SEM and TEM characterizations were carried out, respectively, with a JEOL-JSM5610 SEM and a JEOL JEM-2010F TEM. Elemental analysis was carried out by atomic absorption spectroscopy. Raman spectroscopic analysis was performed with a Renishaw InVia system utilizing a 514.5 nm incident radiation and a 50 × aperture (N.A. = 0.75), resulting in an approximately 2 μm diameter sampling cross section.

2.4. Electrochemical Characterization. Electrochemical performances were evaluated with CR2032 coin cells with an Arbin battery cycler. The coin cells were fabricated with the $LiMPO_4$ or $LiMPO_4$−MWCNT cathode, metallic lithium anode, 1 M $LiPF_6$ in 1:1 diethyl carbonate/ethylene carbonate electrolyte, and Celgard polypropylene separator. The cathodes were prepared by mixing 75 wt % active materials with 12.5 wt % conductive carbon and 12.5 wt % teflonized acetylene black (TAB) binder for $LiFePO_4$ and $LiCoPO_4$ electrodes and 50 wt % active material with 25% conductive carbon and 25% TAB binder for $LiMnPO_4$ because of the very low electronic conductivity of $LiMnPO_4$, rolling the mixture into thin sheets, and cutting them into circular electrodes of 0.64 cm^2 area. The electrodes typically had an active material mass of ∼5 mg and were dried under vacuum at 100 °C for more than 3 h before assembling the cells in an argon-filled glovebox.

3. Results and Discussion

3.1. Synthesis and XRD characterization of $LiMPO_4$. A schematic representation of the MW-ST synthesis process to obtain $LiMnPO_4$, $LiFePO_4$, $LiCoPO_4$, and $LiNiPO_4$ and a subsequent networking with carbon nanotubes to form the $LiMPO_4$-MWCNT nanocomposite are shown in Scheme 1. During the MW-ST process, the microwave induces rotation of the dipoles within the TEG solvent, causing the polar molecules to align and relax in the field of the oscillating electromagnetic radiation. The energy dissipated from the dipole rotations causes the TEG to become hot. Thus, the heat is produced within the liquid and not transferred from the vessel unlike in the conventional autoclave heating

(26) Andrews, R.; Jacques, D.; Rao, A. M.; Derbyshire, F.; Qian, D.; Fan, X.; Dickey, E. C.; Chen, J. *Chem. Phys. Lett.* **1999**, *303*, 467.
(27) Zhang, Z. J.; Wei, B. Q.; Ramanath, G.; Ajayan, P. M. *Appl. Phys. Lett.* **2000**, *77*, 3764.

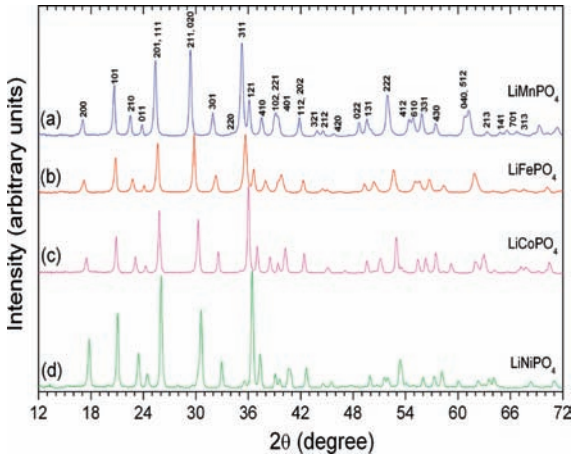

Figure 1. XRD patterns of the $LiMPO_4$ (M = Mn, Fe, Co, Ni) samples prepared by the MW-ST method within 5 to 15 min at 300 °C.

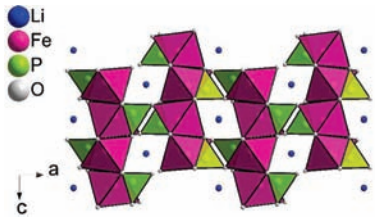

Figure 2. Orthorhombic olivine structure of $LiFePO_4$ projected onto the (010) plane.

methods. This efficient heating leads to an increase in the reaction rates of $LiMPO_4$ formation with improved crystallinity. Subsequent networking of the $LiMPO_4$ with carbon nanotubes at ambient temperatures offers the $LiMPO_4$−MWCNT nanocomposites. The multiwalled carbon nanotube wiring provides the conductive path for electrons at the $LiMPO_4$−MWCNT interfaces.

The XRD patterns of the pristine $LiMnPO_4$, $LiFePO_4$, $LiCoPO_4$, and $LiNiPO_4$ are shown in parts a−d of Figure 1. All of the reflections could be indexed on the basis of the orthorhombic olivine structure (Figure 2) (space group: *Pnma*),[3,14] indicating the formation of phase-pure samples. The sharp diffraction peaks illustrate the highly crystalline nature of $LiMPO_4$ achievable by the MW-ST process within a short reaction time without post annealing at elevated temperatures. The MW-ST method takes advantage of both the microwave irradiation and the solvothermal effect to produce nanocrystalline $LiMPO_4$.

The nonaqueous and viscous solvent (TEG) not only provides a reducing environment to prevent the oxidation of M^{2+} to M^{3+} but also helps to prohibit the growth and agglomeration of the nanoparticles formed. MWCNT is chosen as the conductive additive because of its superior mechanical property, high thermal stability, and good conductivity. The MWCNTs interlace adjacent $LiMPO_4$ nanoparticles together to form a 3D network wiring. The nanoscale networking at ambient temperatures also eliminates the high-temperature processing associated with conventional carbon coating. Moreover, no detectable reflections corresponding to MWCNT could be seen in the XRD patterns of the $LiMPO_4$/MWCNT nanocomposites due to the low content of MWCNT. The XRD peaks in Figure 1 shift

Table 1. Crystallographic Unit cell Parameters of $LiMPO_4$

compound	*a* (Å)	*b* (Å)	*c* (Å)	*V* (Å)
$LiMnPO_4$	10.446	6.106	4.746	302.71
$LiFePO_4$	10.321	6.000	4.695	290.74
$LiCoPO_4$	10.216	5.923	4.704	284.64
$LiNiPO_4$	10.047	5.862	4.681	275.69

gradually to higher angles on going from M = Mn to Fe to Co to Ni due to a decrease in the ionic radius. The lattice parameter values were obtained by refining the XRD data with the *CELREF* software,[28] and they were found to match with the literature values.[6,7,29] Also, the lattice parameters and unit cell volume (Table 1) decrease as we go from M = Mn to Ni in $LiMPO_4$ due to the decreasing ionic radius of the M^{2+} ions. Energy dispersive spectroscopic (EDS) analysis under scanning electron microscopy (SEM) and atomic absorption spectroscopic analysis of the as-synthesized $LiMPO_4$ confirmed a Li/M/P ratio of 1:1:1.

3.2. TEM Characterization of $LiMPO_4$. To better understand the structure and morphology of the $LiMPO_4$ produced, transmission electron microscopy (TEM) observations of all samples were performed (Figure 3). As seen in the first column of Figure 3 (images a, d, g, and j), the synthesis method adopted for $LiMPO_4$ produces nano-thumblike shapes with variations in size and aspect ratio. These nanostructures can be more clearly seen at higher magnifications in the second column of Figure 3 (images b, e, h, and k). In addition, phase contrast high-resolution TEM images of the nano-thumblike structures, which are shown in the third column of Figure 3 (images c, f, i, and l), revealed that each nano-thump is a single crystal for all the four $LiMPO_4$ samples. A more detailed analysis of the high-resolution images and the respective fast Fourier transform (FFT) (an example is shown in images m and n of Figure 3 for $LiMnPO_4$) revealed that all the nano-thumblike $LiMPO_4$ structures exhibit a preferential growth along the [001] direction that is the long axis of the nanothumbs.

In addition, from the diffraction information provided by the FFTs, we could further confirm that the long axis and the width of the nanothumbs correspond respectively to the *c* crystallographic axis [001] and the *a* crystallographic axis [100], whereas the *b* crystallographic axis of the orthorhombic olivine structure (lithium diffusion direction) is parallel to the electron beam direction [010]. Recent computational models and first principle methods on $LiMPO_4$ have shown that, in the orthorhombic olivine structure, the lowest Li^+ migration energy is found for the pathway along the [010] channel, indicating 1D lithium ion mobility along the *b* axis during the charge−discharge process.[30,31] Experimentally, whereas Richardson et al.[32] have observed the movement of Li^+ ions in the *b* direction at the phase boundary by

(28) *Celref for Windows* unit cell refinement program by Laugier J.; Bochu, B. ENSP/Laboratoire des Matériaux etdu Génie Physique, France.
(29) Li, G.; Azuma, H.; Tohda, M. *Electrochem. Solid State Lett.* **2002**, *5*, A135.
(30) Islam, M. S.; Driscoll, D. J.; Fisher, C. A. J.; Slater, P. R. *Chem. Mater.* **2005**, *17*, 5085.
(31) Morgan, D.; Van der Ven, A.; Ceder, G. *Electrochem. Solid-State Lett.* **2004**, *7*, A30.
(32) Chen, G.; Song, X.; Richardson, T. J. *Electrochem. Solid-State Lett.* **2006**, *9*, A295.

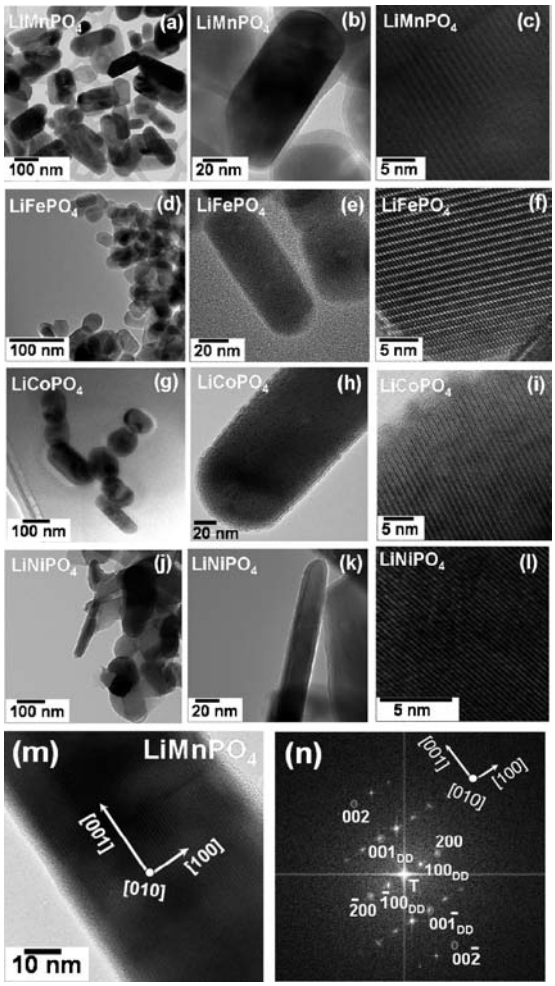

Figure 3. (a)−(m) TEM images of $LiMPO_4$ (M = Mn, Fe, Co, Ni) with nano-thumblike shapes prepared by the MW-ST method within 5 to 15 min at 300 °C. (n) FFT image of the $LiMnPO_4$ shown in image m. The beam direction is B = [010]. The subscript DD refers to double diffraction spots.

electron microscopy, Yamada et al.[33] have pointed out a curved 1D chain for Li^+ ion motion along the [010] direction by combining high-temperature powder neutron diffraction and the maximum entropy method. Consequently, there is enormous interest in synthesizing nanostructured phospho-olivines with the *b* axis along the shortest dimension of the crystallites. The dimensionally modulated, nano-thumblike $LiMPO_4$ presented here by the MW-ST approach exhibits a unique and favorable morphology because the *b* axis is one of the two short dimensions of the nanostructures, resulting in a shorter lithium ion diffusion path length − an important criterion for achieving high-power performance. Similarly, hydrothermal synthesis of $LiFePO_4$ has also been found to display a preferential growth along the [001] direction.[11,21,32]

3.3. Raman Spectroscopic Characterization. On the other hand, Raman spectroscopy is a powerful tool to study the presence of MWCNT in the $LiMPO_4$−MWCNT nanocomposites. Figure 4 shows the Raman spectra of the pristine $LiCoPO_4$, MWCNT, and $LiCoPO_4$−MWCNT nanocomposite. The bands in the 600−1100 cm^{-1} region in part a of

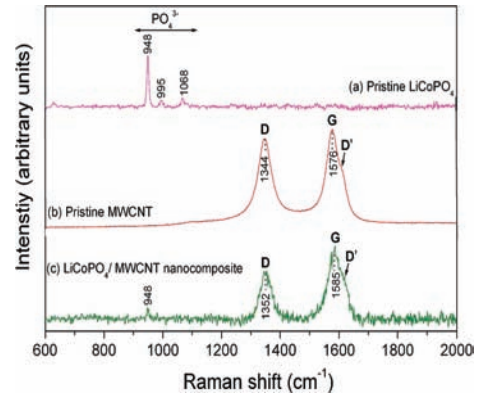

Figure 4. Raman spectra of $LiCoPO_4$ nanothumbs, MWCNT, and $LiCoPO_4$/MWCNT nanocomposite.

Figure 4 corresponds to the intramolecular stretching modes of the PO_4 groups[34] in $LiCoPO_4$. Part b of Figure 4 shows the D and G bands of MWCNT as marked. In the first-order Raman spectra, all graphite-like materials including MWCNT show a strong, sharp peak around 1576 cm^{-1} (G band), which is assigned to the E_{2g} stretching vibration of sp^2 carbon. The other strong, sharp peak at 1344 cm^{-1} (D band) is due to an activation of an otherwise symmetry forbidden set of modes by the defects in the sp^2 network.[35] The exact positions of the bands depend on the laser frequency and the details of the electronic and phonon energy dispersion. The Raman spectrum of the $LiCoPO_4$−MWCNT nanocomposite in part c of Figure 4 shows the characteristic bands for both $LiCoPO_4$ and MWCNT, suggesting the networking of the $LiCoPO_4$ nanothumbs with MWCNT. Moreover, the Raman spectra in parts b and c of Figure 4 exhibit a weak shoulder to the G band toward high wave numbers at 1610 cm^{-1}. This weak shoulder designated as the D′ band has been proposed to occur due to the destruction of carbon nanotubes by chemical oxidation during purification.[36]

3.4. Electrochemical Characterization. Figure 5 compares the discharge capacity at various C rates of the $LiMPO_4$ (M = Mn, Fe, and Co) nanothumbs before and after networking with MWCNT. Figure 6 compares the cyclability of the $LiMPO_4$−MWCNT nanocomposites. An ideal cathode material for lithium ion battery needs to be a mixed ionic and electronic conductor but the olivine-phosphates are both poor electronic and ionic conductors. However, the reduced diffusion length for lithium along one of the short dimensions (*b* axis) in the $LiMPO_4$ nanothumbs enhances the ionic conductance. In addition, the nanoscale networking of the $LiMPO_4$ nanothumbs with MWCNT effectively alleviates the problem of low electronic conductivity by providing a conductive matrix of carbon nanotubes. $LiMnPO_4$ is of particular interest to the battery community because of the ideal location of the $Mn^{2+/3+}$ couple at 4.1 V versus Li/Li^+, which is compatible with the presently available commercial electrolytes.

(33) Nishimura, S. -I.; Kobayashi, G.; Ohoyama, K.; Kanno, R.; Yashima, M.; Yamada, A. *Nat. Mater.* **2008**, *7*, 707.
(34) Julien, C. M.; Zaghib, K.; Mauger, A.; Massot, M.; Salah, A. A.; Selmane, M.; Gendron, F. *J. Appl. Phys.* **2006**, *100*, 063511.
(35) Gupta, A.; Chen, G.; Joshi, P.; Tadigadapa, S.; Eklund, P. C. *Nano Lett.* **2006**, *6*, 2667.
(36) Park, K. C.; Hayashi, T.; Tomiyasu, H.; Endo, M.; Dresselhaus, M. S. *J. Mater. Chem.* **2005**, *15*, 407.

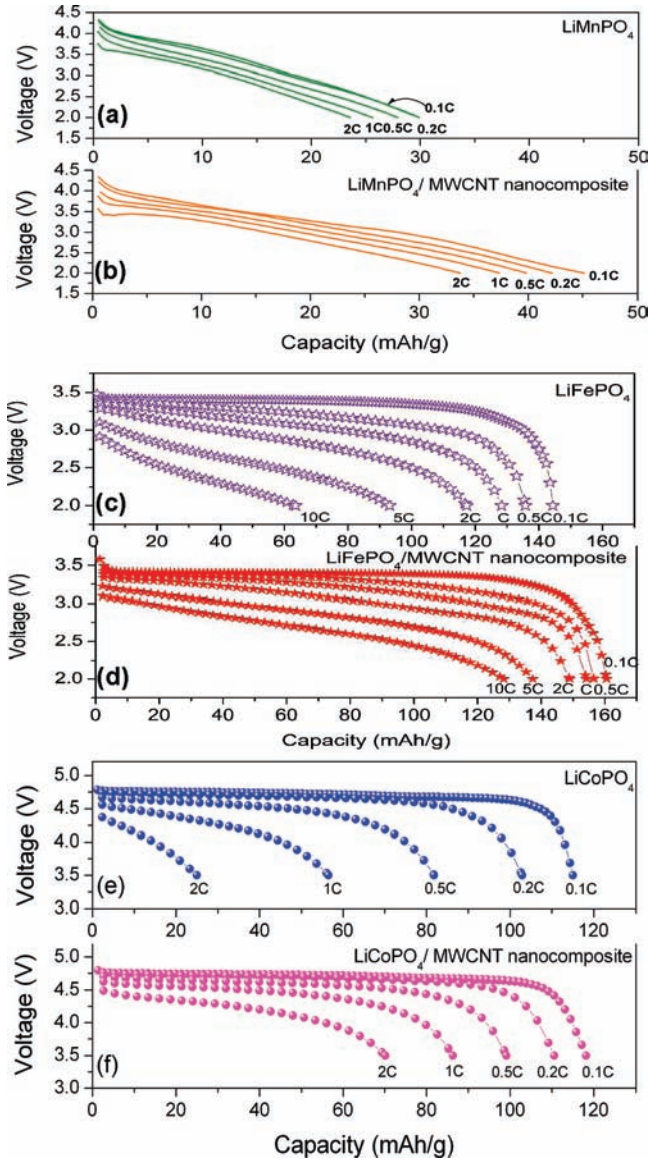

Figure 5. Discharge profiles recorded at different C rates of the pristine $LiMPO_4$ (M = Mn, Fe, Co) prepared by the MW-ST method and the $LiMPO_4$−MWCNT nanocomposites.

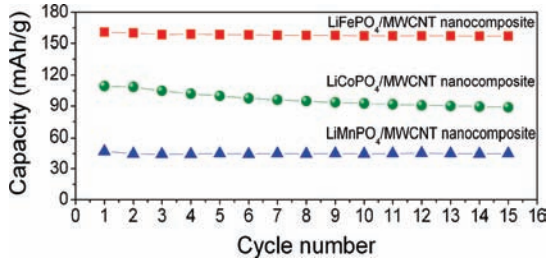

Figure 6. Cyclability data of the $LiMPO_4$−MWCNT (M = Mn, Fe, Co, and Ni) nanocomposites.

However, because of the extremely low intrinsic electronic conductivity ($\sim 10^{-14}$ S/cm) compared to that of $LiFePO_4$ ($\sim 10^{-9}$ S/cm),[37,38] $LiMnPO_4$ exhibits inferior electrochemical performance with a low capacity and a sloping voltage profile arising from a huge polarization loss even at the low C rates of C/10. Although the nano-networking of $LiMnPO_4$ with MWCNT increases the capacity value and improves the cyclability, the capacity value is not comparable to that reported for optimized carbon coated $LiMnPO_4$ nanoparticles,[39,40] and further work on optimization could improve the cell performance.

The $LiFePO_4$ nanothumbs, on the other hand, offer high capacity with excellent power capability, and the $LiFePO_4$−MWCNT nanocomposite exhibits capacities as high as 160 mAh/g at 0.1C rate and retains ~80% of its capacity on going from 0.1C rate to 10C rate. It also exhibits excellent cyclability with no noticeable fade as seen in Figure 6. The rate performance of the $LiFePO_4$−MWCNT nanocomposite is comparable to that found with optimized $LiFePO_4$/C obtained by various synthesis routes in the literature.[18,41] The excellent electrochemical performance exhibited by the $LiFePO_4$−MWCNT sample that was synthesized within a short reaction time (~5 min) without requiring any post annealing is appealing as it can offer significant savings in energy and manufacturing cost.

Realization of near-theoretical capacity in materials like $LiCoPO_4$ that has a higher operating voltage of ~4.8 V can enhance the energy density significantly, which is appealing for next-generation lithium ion cells. However, the $LiCoPO_4$ nanothumbs offer a discharge capacity of only ~120 mAh/g, and the $LiCoPO_4$−MWCNT nanocomposite offers higher rate capability with lower polarization loss compared to the pristine $LiCoPO_4$. We believe the lower capacity value and the capacity fade on cycling (Figure 6) are due to the lack of compatible electrolyte to operate at the high voltage of 4.8 V, and development of more stable electrolyte compositions has the potential to improve the performance of $LiCoPO_4$ further. With a theoretical voltage of 5.1 V versus Li/Li^+, $LiNiPO_4$ poses even a tougher challenge on the electrolyte oxidation issue, and, therefore, we were not able to carry out the electrochemical tests on the synthesized $LiNiPO_4$ nanothumbs with the available conventional electrolytes (1 M $LiPF_6$ in 1:1 diethyl carbonate/ethylene carbonate).

4. Conclusions

In summary, we have demonstrated the synthesis of monodispersed, single-crystalline $LiMPO_4$ (M = Mn, Fe, Co, Ni) with nano-thumblike shapes within a short reaction time (5−15 min) by a novel microwave−solvothermal approach without requiring any elevated temperature post processing in reducing gas atmospheres, significantly lowering the manufacturing cost. Subsequent networking of the $LiMPO_4$ nanothumbs with multiwalled carbon nanotubes at ambient temperatures to give the $LiMPO_4$−MWCNT nanocomposites

(40) Kwon, N-H.; Drezen, T.; Exnar, I.; Teerlinck, I.; Isono, M.; Graetzel, M. *Electrochem. Solid-State Lett.* **2006**, *9*, A277.
(37) Delacourt, C.; Laffont, L.; Bouchet, R.; Wurm, C.; Leriche, J.-B.; Morcrette, M.; Tarascon, J.-M.; Masquelier, C. *J. Electrochem. Soc.* **2005**, *152*, A913.
(38) Sauvage, F.; Baudrin, E.; Gengembre, L.; Tarascon, J.-M. *Solid State Ionics* **2005**, *176*, 1869.
(39) Delacourt, C; Poizot, P.; Morcrette, M.; Tarascon, J.-M.; Masquelier, C. *Chem. Mater.* **2004**, *16*, 93.
(41) Delacourt, C.; Poizot, P.; Levasseur, S.; Masquelier, C. *Electrochem. Solid-State Lett.* **2006**, *9*, A352.

offers high capacity with excellent rate capability. Furthermore, the lithium diffusion direction (*b* axis) along the thickness of the nanothumbs offers particular advantage to achieve fast lithium diffusion and high-power capability necessary for automotive applications.

Acknowledgment. Financial support by the Office of Vehicle Technologies of the U.S. Department of Energy under Contract No. DE-AC02-05CH11231 and Welch Foundation Grant F-1254 is gratefully acknowledged.

IC8015723